Featured in Physics

Capillary-Stress Controlled Rheometer Reveals the Dual Rheology of Shear-Thickening Suspensions

Bruno Etcheverry, Yoël Forterre, and Bloen Metzger*

Aix Marseille Université, CNRS, IUSTI UMR 7343, 13453 Marseille, France

(Received 18 November 2022; revised 15 December 2022; accepted 9 January 2023; published 24 February 2023)

The rheology of dense colloidal suspensions, which may undergo discontinuous shear thickening or shear jamming, is particularly difficult to analyze with conventional rheometers. Here, we develop a rheometer adapted to colloidal suspensions: the "capillarytron," which uses the air-suspension capillary interface to impose particle (or osmotic) pressure during shear. The main virtues of this new device are that (i) it gives direct access to the suspension friction coefficient, (ii) it operates for very dense suspensions up to jamming, and, most importantly, (iii) it decouples the stresses developed within the suspension from the applied shear rate. We can, thus, smoothly move through the different frictional states of the system, precisely in the range of volume fractions where discontinuous shear thickening or shear jamming occur under volume-imposed conditions. Our results obtained with the capillarytron provide the first complete characterization of the dual frictional behavior of a model shear-thickening suspension, in agreement with the recently proposed frictional transition scenario. Based on a new concept in rheometry, the capillarytron unlocks the path to pressure-imposed rheology on colloidal and Brownian suspensions. Moreover, its fine control of the particle pressure via the soft capillary interface opens the possibility to explore the flow of "fragile" particles close to jamming, such as Brownian colloids, active particles, and living cells.

DOI: 10.1103/PhysRevX.13.011024 Subject Areas: Fluid Dynamics, Soft Matter

I. INTRODUCTION

During the past decade, a large consensus has grown about the central role played by frictional particle contacts in dense colloidal suspensions. This turnabout has led to major advances in the field. In particular, the discontinuous shear-thickening rheology of certain dense suspensions [1–3], which long remained a puzzle, can now be simply understood and rationalized as a frictional transition [4–6]. The suspension thickens beyond a critical stress that is necessary to push the particles, repulsive in nature, into frictional solid contact. Considering the importance of solid contacts also led to the emergence of new research areas. One of them is the possibility now to control the suspension rheology while in application, either by means of a biaxial shear [7], by applying external vibrations [8,9], or by thermal action [10]. These external levers can be used *in situ* to lower the fraction of frictional contacts, which dramatically decreases the suspension viscosity. Another emerging field, with many exciting application opportunities, relies on engineering of the particle surface properties so that specific rheological characteristics are imparted to the suspension. This can be done by tuning the roughness and/or friction of the particles at the nanoscale [11–13] or by controlling the nature of the interparticle interactions with custom polymer coatings or repulsive electrostatic charges [14,15]. Along this line of research, the adjunction of superplasticizers in the formulation of modern concretes, which long remained completely empirical, is now also interpreted within the frictional transition framework [16,17].

The above examples highlight the close link between *tribology* and *rheology* in colloidal suspensions: The nature of particle-to-particle contacts at the nanoscale is crucial to understand and potentially control the macroscopic rheological behavior of suspensions. This recent breakthrough is currently the subject of intense research. However, it suffers from the lack of appropriate rheological tools to diagnose the frictional behavior of colloidal suspensions.

The interparticle friction coefficient μ_p and the suspension friction coefficient μ are now important quantities one needs to access. Classical or advanced AFM techniques have been used to probe the interparticle friction coefficient μ_p [11,15,18–20]. However, complete *in situ* characterization of the suspension friction coefficient μ, which directly reflects the frictional state of the particles [21,22], remains inaccessible. Conventional rheological techniques, which are performed under fixed volume fraction ϕ, provide

*Corresponding author.
bloen.metzger@univ-amu.fr

information on the shear rate $\dot{\gamma}$, shear stress τ, and shear viscosity η but give no indication on the suspension frictional state. The suspension friction coefficient $\mu = \tau/P_p$ is defined, by analogy with Coulomb friction law, by the ratio of the tangential shear stress τ over the particle pressure P_p [23,24]. Particle pressure is generally defined as the mean normal stress exerted by the particle phase in a sheared suspension and is shown to be equivalent to a nonequilibrium osmotic pressure [25,26]. An alternative definition considers the vertical (i.e., in the direction of the velocity gradient) normal component of the particle stress tensor, which is the definition generally used to access the friction coefficient in dense granular flows [27] or non-Brownian suspensions [23]. The suspension friction coefficient μ can be measured in P_p-imposed configurations. However, the existing P_p-imposed rheometers [23,28,29] are not suited to colloidal suspensions, as particles must have a diameter greater than a few hundred microns. The rotating drum [30] or the inclined plane [31] configurations have been used to highlight the frictional transition at the origin of shear thickening. However, both of these configurations do not allow to vary the particle pressure, which is there set by gravity. An original rheological configuration, using a transverse Darcy fluid flow to control the particle pressure, was developed recently [32], but it is limited to the study of the quasistatic regime.

In this study, we introduce a new rheometer: the capillarytron, which through direct control of the granular pressure gives access to the frictional constitutive laws of colloidal suspensions. This device is based on a new concept in rheometry, since to impose the particle pressure, instead of using a rotating rigid grid as in Boyer, Guazzelli, and Pouliquen [23], here the particle pressure is imposed by the capillary air-suspension interface. After presenting the concept of this new rheometer, we first validate its application by studying a (non-shear-thickening) suspension of macroscopic frictional spheres, whose rheology is already well documented [24]. We then investigate the frictional rheology of a model shear-thickening suspension of non-Brownian silica microparticles, for which frictional contacts and short-range repulsive interactions are simultaneously at play. These results reveal that the suspension frictional behavior strongly depends on the applied particle pressure, in agreement with the frictional transition scenario recently proposed to explain shear thickening in colloidal suspensions [4–6]. In addition, we provide the first full characterization of the frictional constitutive laws of such a suspension and further explore the frictional signatures of different colloidal suspensions, testing the capabilities of the capillarytron on Brownian and more complex shear-thickening suspensions.

II. RESULTS

A. Capillarytron: The concept

The concept of the capillarytron stems from an intrinsic property of particulate suspensions, namely, that, under shear, particulate suspensions are dilatant [2,3]. This means that sheared suspensions spontaneously develop particle normal stresses σ_p, which deforms the capillary air-suspension interface [33], thereby inducing a negative liquid pressure P_ℓ [26,34]. The concept of the capillarytron lies in reversing this situation, precisely by controlling the liquid pressure in order to impose particle pressure.

A sketch of the capillarytron is shown in Fig. 1(a). It is based on a classical plane-plane rheometric configuration where the suspension is sheared between two rough disks of radius $R = 25$ mm spaced by a variable gap of height h. The upper plane is driven in rotation by an Anton Paar DSR 502 rheometer head which allows us to control the shear stress τ. One first originality of this device is that the lower plane is porous. Made out of a rigid grid covered with a fine mesh smaller than the particle diameter, the bottom plane is permeable to the suspending fluid, which can then be directly connected to a reservoir of adjustable height H. By varying the height of this reservoir, we have control on the liquid pressure $P_\ell = -\rho_\ell g H$ within the sample, where ρ_ℓ is the liquid density and g denotes gravity. During shear, the steady-state radial force balance at the capillary interface prescribes that

$$\sigma_p^r(R) + P_\ell = 0, \tag{1}$$

where $\sigma_p^r(R)$ is the radial particle pressure at the capillary interface; see Fig. 1(b). Controlling the liquid pressure thus allows us to impose radial particle stress. Instead of using a rigid moving grid as in Boyer, Guazzelli, and Pouliquen [23], the capillarytron uses the capillary air-suspension interface to control the particle stress. This is a key aspect that makes the capillarytron suited to colloidal suspensions. Indeed, the maximum particle pressure that a capillary interface can sustain is typically $10\gamma/d$ [2,35], where γ is the fluid surface tension and $10/d$ is the maximal curvature of the capillary interface between grains. For instance, taking $\gamma \approx 70$ mN.m^{-1} for water and particles of diameter $d = 10$ μm, the maximum imposed particle pressure can reach 7×10^4 Pa, which corresponds to the pressure of a water column of 7 m. In practice, the imposed pressure remains in the range $P_\ell \in [5\text{–}1000]$ Pa or, equivalently, $H \in [0.5\text{–}100]$ mm.

The second important feature of this device is that the bottom part of the setup rests on a precision scale used as a vertical force sensor. The measured mass m (which is set to zero for the suspension at rest, i.e., for $\dot{\gamma} = 0$) results from the contributions of both the mean vertical particle pressure $\bar{\sigma_p^z}$ and the liquid pressure P_ℓ, such that

$$mg = (\bar{\sigma_p^z} + P_\ell)\pi R^2. \tag{2}$$

Note that this thrust is related to the normal stress differences [36]. From the value of the liquid pressure P_ℓ

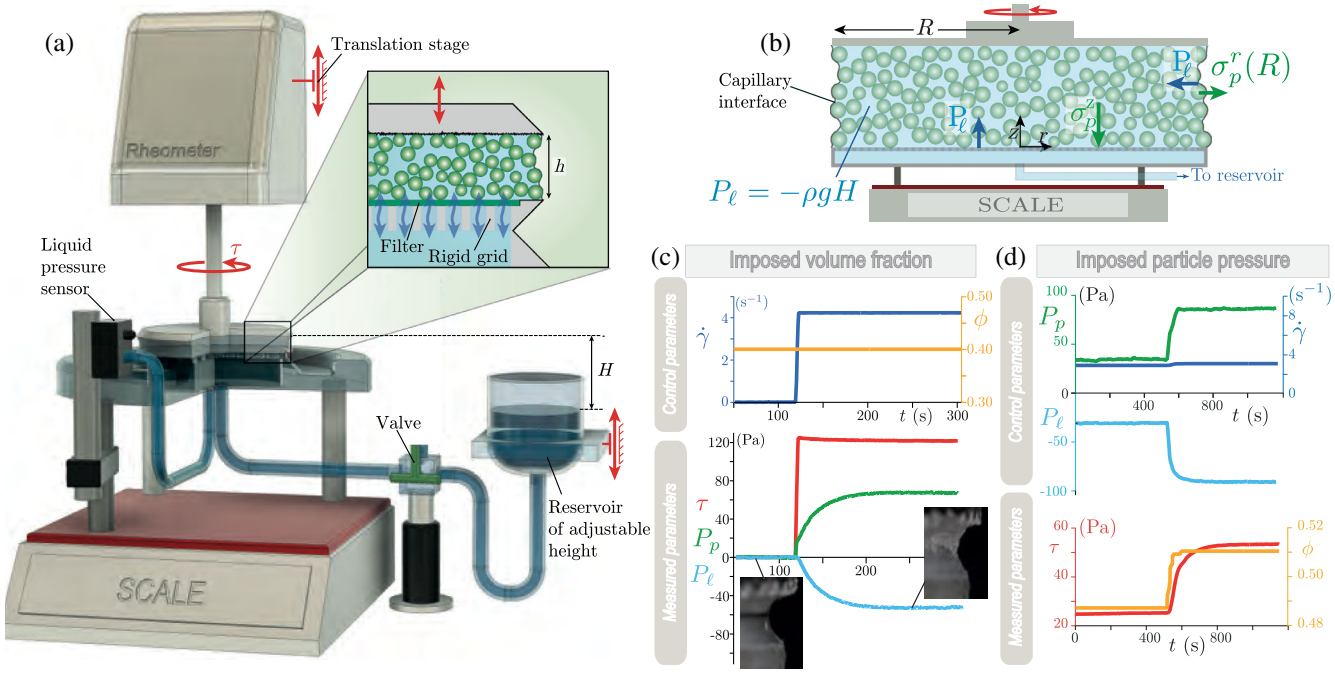

FIG. 1. Capillarytron: The concept. (a) Sketch of the capillarytron. A reservoir of adjustable height is connected to the suspension through a permeable grid to impose a negative liquid pressure $P_\ell = -\rho g H$: Here, the capillary interface is used to impose the particle pressure. (b) Schematic of the horizontal and vertical force balances in steady state: In the radial direction and at the air-suspension capillary interface, the particle pressure $\sigma_p^r(R)$ is balanced by the liquid pressure P_ℓ. In the vertical direction, the mass m measured with the scale results from the contribution of the mean particle stress in the vertical direction $\bar{\sigma}_p^z$ and the liquid pressure P_ℓ. (c) Typical experiment under volume-imposed condition (valve closed). The liquid pressure becomes negative as a result of the particle stress developed by the dilatant suspension. Images of the smooth and corrugated capillary interface before and during shear, respectively. (d) Typical experiment under pressure-imposed condition (valve open). Under constant shear rate and upon a sudden increase of particle pressure obtained by lowering the reservoir, the shear stress and the volume fraction self-adjust to a new steady state.

(imposed with the reservoir) and the mass m (measured with the scale), one can easily access the mean vertical particle pressure $\bar{\sigma}_p^z$, which corresponds to the particle pressure $P_p \equiv \bar{\sigma}_p^z$ needed to characterize the frictional rheological laws $\mu(J) = \tau/P_p$ and $\phi(J)$, where $J = \eta_\ell \dot{\gamma}/P_p$ is the viscous number characterizing the flow under pressure-imposed conditions, with η_ℓ the fluid viscosity [24].

The capillarytron, thus, builds on a lineage of experimental apparatus, inspired by that of Prasad and Kytömaa [28], who provided the first direct measurement of the particle pressure using a mobile grid, as in the configuration proposed later by Boyer, Guazzelli, and Pouliquen [23]. We also leverage the concept of fluid or "grid-pressure" measurement [26,34,37] giving access to the particle normal stress from the simultaneous measurement of the total normal stress and the liquid pressure. The capillarytron conceptually goes a step further, as the fluid or grid pressure is here not only measured, it is used as a control parameter to impose the particle pressure. For the sake of clarity, note also that Prasad-Kytömaa [28] and Boyer-Guazzelli-Pouliquen [23] configurations impose the vertical component of the particle pressure σ_p^z, while we impose the vorticity (radial) component of particle pressure σ_p^r.

The dilatant nature of suspensions and the forces resulting from this dilation can be well illustrated under fixed volume conditions; see Fig. 1(c). Here, the valve is used to close the connection between the suspension and the reservoir: The suspension volume fraction ϕ is then imposed. We start from rest ($\dot{\gamma} = 0$) and set to zero both the fluid pressure and the mass. For this reference initial condition, the air-suspension interface is smooth; see Fig. 1(c). Upon increasing the suspension shear rate $\dot{\gamma}$ to a finite value, the dilatant suspension develops positive particle stresses which corrugate the air-suspension interface. As a result, the liquid pressure P_ℓ inside the sample becomes negative. The values of P_p, P_ℓ, and τ can be used to compute the suspension friction coefficient $\mu(J) = \tau/P_p$ and $J = \eta_\ell \dot{\gamma}/P_p$ for the reached steady-state condition.

The main novelty and strength of the capillarytron lie in giving the possibility to invert controlled and measured parameters relative to the above volume-imposed conditions. Opening the valve switches the capillarytron to pressure-imposed conditions where adjusting the height H of the reservoir gives control on the particle pressure. The control parameters are now $\dot{\gamma}$ and P_p, while the volume fraction ϕ is free to adjust. Figure 1(d) shows how the

suspension evolves under a constant applied shear rate and under a step increase of particle pressure, obtained by suddenly lowering the height H of the reservoir. We observe that the volume fraction ϕ and the shear stress self-adjust until reaching a new steady state satisfying Eqs. (1) and (2). Importantly, change of the volume fraction induces a change of the volume of the sample, which we accommodate by changing the gap h in order to maintain constant the particle pressure [38]. The value of h is then used to compute the evolution of the suspension volume fraction, given that $\phi = V_p/\pi R^2 h$, where V_p denotes the initial and constant volume occupied by the particles.

B. The capillarytron: Proof of concept

As a first test of the capabilities of the capillarytron, we start by investigating a classical (non-shear-thickening) suspension of macroscopic frictional particles. The suspension is composed of macroscopic PMMA particles [$d = 120$ μm; see Fig. 2(a)] immersed in a Newtonian and viscous liquid (Tritton X100) of viscosity $\eta_\ell = 0.27$ Pa.s. In this case, particles interact only through hydrodynamics and frictional solid contacts. The rheology is, thus, rate independent, and the frictional laws $[\mu(J), \phi(J)]$ of such a suspension are well documented [23] and depend on a unique dimensionless number $J = \eta_\ell \dot{\gamma}/P_p$ [24] [see Fig. 2(b) for the definition of the relevant variables]. In Fig. 2(c), we show the constitutive laws obtained with the capillarytron under imposed particle pressure and varying J using either successive steady decreasing values of shear rates or a quasisteady decreasing ramp of shear rate for a gap $h \in [2.5\text{–}3.5]$ mm (see the Appendix for details on the protocols). The data obtained can be very well fitted by the simple expressions $\mu(J) = \mu_c + AJ^{\alpha_\mu}$ and $\phi(J) = \phi_J/(1 + BJ^{\alpha_\phi})$, giving parameters $\mu_c = 0.30$, $A = 2.99$, $\alpha_\mu = 0.50$, $\phi_J = 0.57$, $B = 1.10$, and $\alpha_\phi = 0.45$, which are in good agreement with previous measurements [23] and theoretical predictions [22] for such a frictional granular suspension. Both insets, showing the reduced macroscopic friction coefficient $\Delta\mu = \mu - \mu_c$ and the change of volume fraction relative to jamming $\Delta\phi = \phi_J - \phi$ versus J, indicate that the dynamic contribution to the frictional laws can be well approximated by simple power-law functions over a very large range (more than six decades) of the viscous number J.

To anticipate on the following, two major features of the frictional behavior of this (non-shear-thickening) suspension must be highlighted. First, the quasistatic friction coefficient obtained for vanishing J (at jamming), $\mu_c = 0.30$, is a direct indication that the suspension is composed of frictional particles [21,22]. Second, we observe that measurements performed under different applied particle pressures ($P_p = 10$ or 100 Pa) collapse on a single master curve $\mu(J)$. This collapse shows that the rheology of a suspension of macroscopic frictional particles is independent of the applied particle pressure P_p, which, as shown next, is not the case for shear-thickening suspensions.

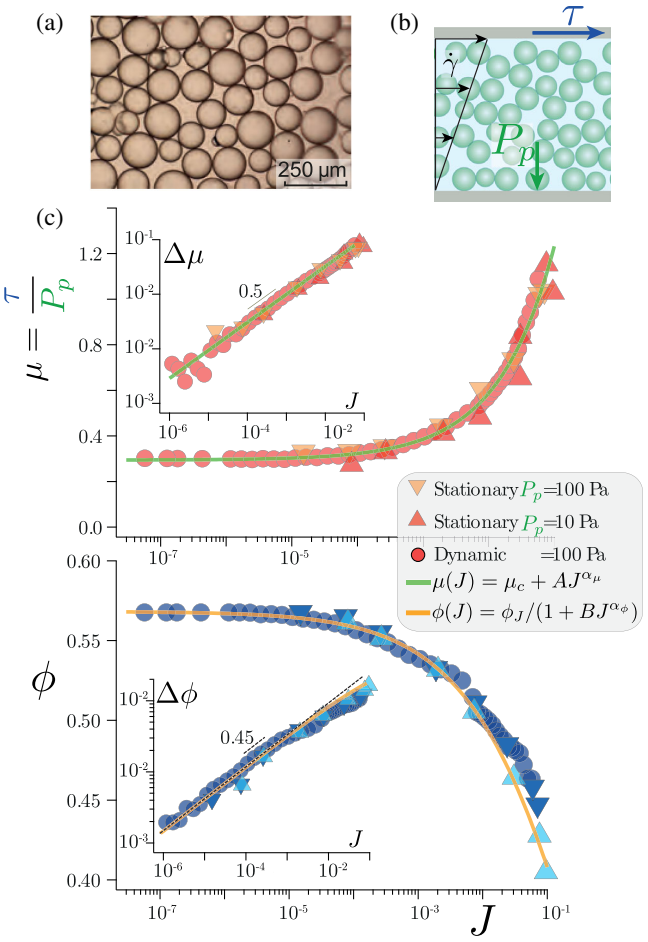

FIG. 2. Capillarytron: Proof of concept on a Newtonian suspension. (a) Picture of the PMMA particles of diameter $d \approx 120$ μm. (b) Relevant variables to access the frictional rheology: shear stress τ, particle pressure P_p, and shear rate $\dot{\gamma}$. (c) Frictional rheological laws. Top: suspension friction coefficient $\mu = \tau/P_p$; bottom: suspension volume fraction ϕ versus viscous number $J = \eta_\ell \dot{\gamma}/P_p$, obtained from stationary and quasisteady "dynamic" ramps of shear rate. The data are fitted by $\mu(J) = \mu_c + AJ^{\alpha_\mu}$ and $\phi(J) = \phi_J/(1 + BJ^{\alpha_\phi})$ with $\mu_c = 0.30$, $A = 2.99$, $\alpha_\mu = 0.50$, $\phi_J = 0.57$, $B = 1.10$, and $\alpha_\phi = 0.45$. Insets: (top) reduced macroscopic friction coefficient $\Delta\mu = \mu - \mu_c$ and (bottom) reduced volume fraction $\Delta\phi = \phi_J - \phi$ versus J.

C. Frictional rheology of a model shear-thickening suspension

After validating the proof of concept of the capillarytron on a Newtonian suspension, we now turn to the study of a model shear-thickening suspension composed of silica particles of much smaller diameter $d = 23.46 \pm 1.06$ μm; see Fig. 3(a). When immersed in a water solution, these silica particles spontaneously develop an electrostatic double layer, which generates an electrostatic repulsive pressure between the grains $P_{\text{rep}} = F_0 e^{-r/\lambda_D}/d^2$, where

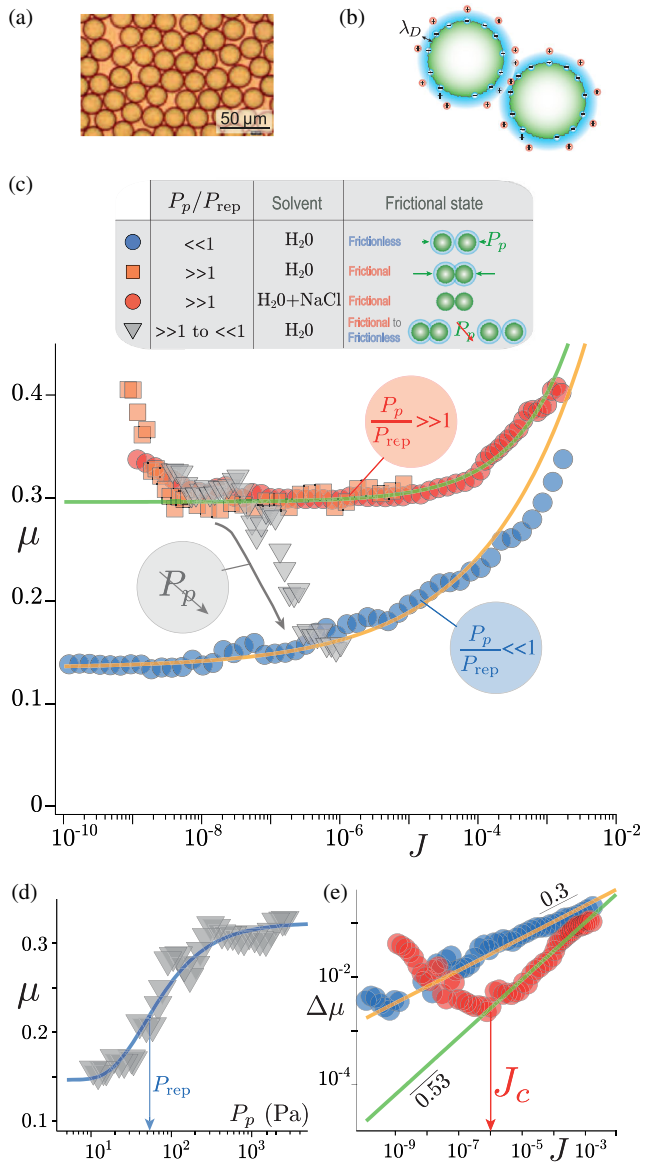

FIG. 3. Frictional rheology of a model shear-thickening suspension. (a) Picture of the silica particles, $d = 23.46 \pm 1.06$ μm. (b) Schematic illustrating the electrostatic double layer at the origin of the short-range repulsive force and the Debye length λ_D. (c) Macroscopic friction coefficient μ versus J for measurement performed at low particle pressure ($P_p = 5$ Pa, $P_p \ll P_{rep}$), at large particle pressure ($P_p \approx 500$ Pa, $P_p \gg P_{rep}$), in a solution of water and NaCl ($[NaCl] = 0.2$ mol.L^{-1}, $P_p \gg P_{rep}$), and for a decreasing ramp of particle pressure ($P_p = 2600$ to 10 Pa, $P_p \gg P_{rep}$ to $P_p \ll P_{rep}$). (d) Macroscopic friction coefficient μ versus P_p for the decreasing ramp of particle pressure shown in (c). (e) Reduced macroscopic friction coefficient $\Delta\mu = \mu - \mu_c$ versus J from data shown in (c) (the same symbols). Solid lines: fittings of the data by $\mu = \mu_c + AJ^{\alpha_\mu}$.

$F_0/d \sim 1$ mN/m [39], r is the interparticle separation distance, and $\lambda_D = 0.304\ \text{nm}/\sqrt{[NaCl]}$ is the Debye length, which can be tuned by varying the ionic solvent concentration [NaCl]; see Fig. 3(b). Typically, the repulsive pressure between particles is 50 Pa in pure water, but it can be completely screened simply by adding salt above the ionic concentration of 0.1 mol.L^{-1} [30]. Previous studies on the frictional behavior of this suspension of silica particles are limited to the quasistatic regime ($J \to 0$) [30,32] or to fixed particle pressure conditions [30,31]. The major contribution of the capillarytron here is that we can now explore the suspension frictional behavior with the possibility of varying J, P_p, and P_{rep} independently. This represents ideal conditions, as the suspension friction coefficient should now depend on the two dimensionless number J and P_p/P_{rep} [6,32].

Figure 3(c) shows the suspension friction coefficient μ versus J obtained with different protocols. We perform isopressure measurements, varying J by changing the shear rate $\dot{\gamma}$ but keeping a constant particle pressure by fixing the reservoir height. The blue-circle curve corresponds to measurements performed under a very low imposed particle pressure of 5 Pa (i.e., 10 times smaller than the critical repulsive pressure) such that $P_p/P_{rep} \ll 1$. The obtained frictional curve has an overall very low friction coefficient. Indeed, when fitted by the expression $\mu(J, P_p/P_{rep} \ll 1) = \mu_c + AJ^{\alpha_\mu}$, the obtained quasistatic friction coefficient $\mu_c = 0.13$, very close to 0.1, indicates that particles behave essentially as frictionless grains [30,31,40].

For the orange-square and red-circle curves, we explore the opposite limit $P_p/P_{rep} \gg 1$. This can be achieved in two different ways: either by increasing P_p up to 500 Pa (by lowering the position of the reservoir) or by screening the repulsive pressure using a water/NaCl solution of concentration $[NaCl] = 0.2$ mol.L^{-1} for the suspending fluid. Strikingly, both protocols lead to the same frictional branch having an overall much larger friction coefficient. These results not only highlight the frictional transition, they also show explicitly that the dimensionless number controlling this transition is P_p/P_{rep}. Fitting these frictional curves results in $\mu_c = 0.3$, a value similar to that obtained previously with the suspension of macroscopic frictional particles [see Fig. 2(c)]. These results highlight the extreme frictionless and frictional branches obtained for $P_p/P_{rep} \ll 1$ and $P_p/P_{rep} \gg 1$, respectively. Finally, we can also move throughout the frictional transition by progressively decreasing P_p from above to below P_{rep}. This leads to a smooth transition from the frictional to the frictionless curves (gray triangles), indicating that a continuum of frictional states exists between the two extreme frictionless and frictional branches obtained with the previous protocols. The same data (gray triangles) plotted versus P_p [Fig. 3(d)], when fitted in the spirit of the Wyart-Cates model [6,41] as $\mu(P_p/P_{rep}) = \mu_0(1-f) + \mu_1 f$ with $f = e^{-P_{rep}/P_p}$, yields $P_{rep} = 47$ Pa, in close agreement with the expected critical repulsive pressure in pure water [30]. Note that the frictional transition model also predicts a continuum of curves $\phi(J, P_p/P_{rep})$ between the frictionless

and frictional branches. However, for this suspension of small particles (gap $h \sim 300$ μm), we are not able to accurately resolve the small relative changes in ϕ, which are of the order of a few percent, as opposed to changes of more than 200% for μ when shifting from frictionless to frictional.

In addition to providing direct validation of the frictional transition model for this shear-thickening suspension, the capillarytron reveals two other major features of its frictional behavior. First, it offers sufficient resolution to highlight that the constitutive laws of frictionless and frictional particles do not follow the same power law of J. As shown in Fig. 3(e), the reduced macroscopic friction coefficient $\Delta\mu = \mu - \mu_c$ follows a power law of J with an exponent $\alpha_\mu \approx 0.3$ for frictionless grains (blue circles) and $\alpha_\mu \approx 0.53$ when friction is activated (red circles), in good agreement with previous measurements [31] and theoretical predictions [22]. Second, while the frictionless curve $\mu(J, P_p/P_{\text{rep}} \ll 1)$ follows a monotonic trend with J, the frictional curve $\mu(J, P_p/P_{\text{rep}} \gg 1)$ is clearly nonmonotonic and presents a minimum around $J_c \approx 10^{-6}$ [Fig. 3(e)]. This nonmonotonic trend is suggested by previous measurements of the avalanche angle in a rotating drum [31]. However, here, by allowing control of the applied shear rate, the capillarytron gives direct access to the unstable velocity-weakening part of the flow curve.

D. Toward more complex colloidal suspensions

To complete demonstrating the capillarytron's versatility, we turn to more complex colloidal suspensions. Figure 4(a) shows the suspension friction coefficient μ of a suspension of slightly Brownian silica particles of diameter $d = 4.7$ μm, obtained for an imposed particle pressure $P_p = 20$ Pa that is well below the repulsive pressure $P_{\text{rep}} \approx 250$ Pa, estimated by assuming that the repulsive force is proportional to d [39]. The curve reaches $\mu_c \simeq 0.08$ when $J \to 0$, indicating that grains behave as frictionless particles as expected under this low level of pressure. Interestingly, for this system and for the low-J value investigated ($J \in [10^{-10}$–$10^{-2}]$), the ratio between the particle pressure and the thermal pressure, $\tilde{\Pi} = P_p d^3/k_B T \sim 10^5$, is close to the thermal crossover [42]. The measured μ_c value slightly below the 0.1 athermal limit could thus be the signature of a frictional weakening due to Brownian motion [43,44]. We conclude by investigating the frictional behavior of a shear-thickening suspension of potato-starch particles immersed in water [Fig. 4(b)]. The additional complexity of this suspension comes from the particle polydisperse size and nonspherical shapes. Particles also interact through a repulsive force of different origin, stemming from the deployment of hydrophilic carbohydrate polymers at the particle surface. Nonetheless, we are able to identify two very distinct frictional branches at low ($P_p = 10$ Pa) and large ($P_p = 500$ Pa) particle pressure, which encompasses the

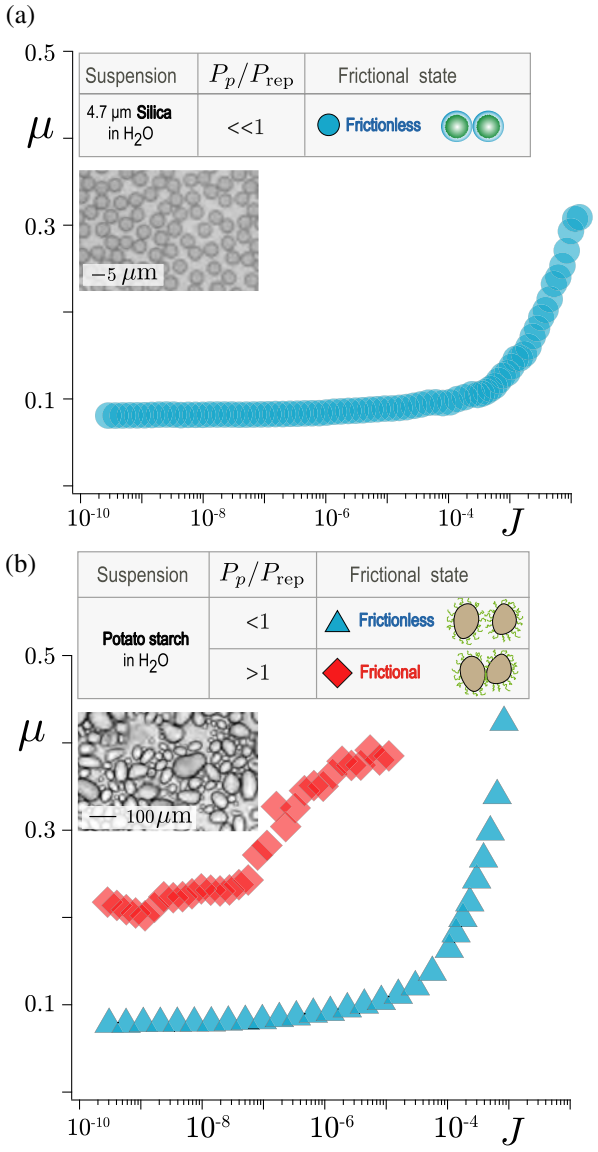

FIG. 4. Toward more complex colloidal suspensions. Suspension friction coefficient μ versus viscous number J (a) for a suspension of slightly Brownian silica particles of diameter $d = 4.7$ μm immersed in water and measured at $P_p = 20$ Pa ($P_p/P_{\text{rep}} \ll 1$) and (b) for a suspension of potato-starch particles immersed in water and measured at small ($P_p = 10$ Pa, $P_p/P_{\text{rep}} \ll 1$) and large ($P_p = 500$ Pa, $P_p/P_{\text{rep}} \gg 1$) particle pressure.

critical repulsive pressure $P_{\text{rep}} \approx 100$ Pa estimated from the onset shear stress for discontinuous shear-thickening $\tau^* \approx 10$ Pa using $P_{\text{rep}} = \tau^*/\mu$ with $\mu \approx 0.1$. To our knowledge, this is the first experimental evidence of the frictional transition on this complex, yet emblematic, shear-thickening suspension.

III. DISCUSSION

Motivated by the recent understanding of shear thickening [4–6] and the numerous evidences of the preponderant

role of interparticle frictional contacts in colloidal suspensions, we develop a new rheometer: the capillarytron, capable of probing *in situ* the frictional behavior of these suspensions. The capillarytron is based on an original concept in rheometry: By controlling the pressure of the liquid phase within the suspension, the air-suspension capillary interface can be put under tension on the grains in a controlled manner. This technique not only allows very precise control of granular pressure (<1 Pa), but it also has the advantage of being applicable to very small grains. We show its capabilities in the micrometric particle size range, but there is actually no fundamental limit to further extend the technique to submicronic particle sizes by adapting the bottom plate filter.

A first key feature of the capillarytron is that it operates under imposed particle pressure, which is a major advantage, as this configuration decouples the shear rate from the stresses developed within the suspension. Under volume-imposed conditions, discontinuous shear thickening or shear jamming are very difficult to study with conventional rheometers as increasing the shear may cause divergence of the stresses and of the suspension viscosity. By contrast, with the capillarytron, the particle stress is imposed independently from the shear rate. We can, thus, smoothly move through the different frictional states of the suspension. We leverage this capability to provide the first experimental comprehensive view of the frictional behavior of a shear-thickening suspension, documenting both its quasistatic ($J \to 0$) and dynamic ($J > 0$) regimes. Our results explicitly show that the presence of a repulsive force between the particles induces the existence of a frictionless state of the particles at low granular pressure ($P_p \ll P_{\mathrm{rep}}$), while under large pressure or, equivalently, when the repulsive force between the particles is lowered ($P_p \gg P_{\mathrm{rep}}$), the suspension becomes frictional. The frictional transition model proposed by Wyart and Cates in 2014 to explain the shear thickening is here directly evidenced by varying the ratio P_p/P_{rep}.

Another strong asset of the capillarytron is the wide range of viscous number it can access, reaching values as small as $J \sim 10^{-10}$. This allows us to precisely determine the critical exponent of the constitutive laws, for both frictionless and frictional particles, confirming previous theoretical and numerical predictions. We also directly observe the "velocity-weakening" behavior of the frictional branch at low J, a phenomenon which emerges only at viscous number values J lower than 10^{-6}. For comparison, the most advanced discrete element method numerical simulations today can hardly reach viscous numbers lower than 10^{-5} [22,45].

Overall, the capillarytron provides a unique means to probe *in situ* the frictional behavior of dense suspensions and access information about particle interactions that are usually inaccessible in conventional rheometry. The quasistatic friction coefficient μ_c measured with the capillarytron is a robust quantity, which can be directly related to the value of the interparticle friction coefficient [21,22,29], including or not rolling friction [46,47], and which can be decoupled from adhesive effects by changing P_p. It is also a more reliable proxy of microscopic friction than the critical volume fraction ϕ_c at which the suspension jams, as ϕ_c only weakly depends on μ_p and can be strongly affected by finite range repulsive interactions, particle elasticity, or adhesion effects. The capillarytron, therefore, appears to be the ideal tool to quantify the effect of surface coating or controlled roughness, which are presently synthesized in many different research groups [10,11,15]. Finally, by independently controlling the particle pressure and shear rate through a "soft" capillary interface, the suspension rheology can be investigated at very high-volume fractions while maintaining harmless confining pressures. The capillarytron, thus, opens the possibility to explore the flow of "fragile" particles close to jamming, such as Brownian colloids, active particles [48], and living cells [49].

ACKNOWLEDGMENTS

We thank O. Pouliquen for fruitful discussion and his suggestion of using a capillary interface to control the particle pressure, S. Noel for his help in building the capillarytron, and W. Lecoz for the Labview interface. This work was supported by the European Research Council (ERC) under the European Union Horizon 2020 Research and Innovation program (ERC Grant Agreement No. 647384) and by ANR *ScienceFriction* (ANR-18-CE30-0024).

APPENDIX: MATERIALS AND METHODS

1. Particles

The silica particles used in Figs. 3 and 4 are commercial particles from Microparticles GmbH with diameter $d = 23.5$ and 4.7 μm, respectively, and both of density $\rho_p = 1850\ \mathrm{kg\,m^{-3}}$. Before each experimental campaign, the silica particles are cleaned in Piranha solution (1:2 of H_2O_2: H_2SO_4) for 10 min and then rinsed several times with pure microfiltered water. They are then immersed in the desired ionic solution, placed in an ultrasonic bath for 10 min, and rinsed 4 times with the ionic solution. After testing that the suspending fluid conductivity corresponds to the desired ionic concentration, the grains are immediately used in the shear cell.

2. Preparation of the initial pressure-imposed steady state

We used both steady-state measurements as shown in Fig. 1(d) and dynamic ramp measurements. Both protocols require the preparation of an initial pressure-imposed steady state, which is done as follows: (i) With the valve closed (imposed volume), the suspension initially prepared at 40% is placed in the plane-plane shear cell. (ii) The valve

that connects the sample to the reservoir is opened, and the height of the reservoir H is adjusted to the level of the sample so that the tank and the sample are in hydrostatic equilibrium with a straight meniscus. We wait 30 s, to ensure that there is no more liquid flow between the reservoir and the sample. We choose this tank height as the height reference for H and, concomitantly, the balance is set to zero, and we adjust the altitude of the pressure sensor to obtain $P_\ell = 0$. The references of height, mass, and liquid pressure are made. (iii) A ramp in shear rate is then started during which the suspension is progressively pressurized by lowering the reservoir. Once the desired initial shear rate is reached, H is finely tuned to adjust the particle pressure. (iv) Once the initial steady state is reached, we can start the measurement.

3. Dynamic ramp protocol

(i) From an initial pressure-imposed stationary state, a slowly descending ramp of shear rate is applied under constant pressure (constant H). (ii) During the ramp, the viscous number $J = \eta_\ell \dot{\gamma}/P_p$ decreases, because the shear rate decreases at constant particle pressure. As the volume fraction gradually increases, the gap h is decreased in order to keep the particle pressure constant. Typically, the gap h is decreased in steps of 1 μm, which does not significantly perturb the measurement.

[1] H. Freundlich and H. Röder, *Dilatancy and Its Relation to Thixotropy*, Trans. Faraday Soc. **34**, 308 (1938).

[2] E. Brown and H. M. Jaeger, *The Role of Dilation and Confining Stresses in Shear Thickening of Dense Suspensions*, J. Rheol. **56**, 875 (2012).

[3] E. Brown and H. M. Jaeger, *Shear Thickening in Concentrated Suspensions: Phenomenology, Mechanisms and Relations to Jamming*, Rep. Prog. Phys. **77**, 046602 (2014).

[4] R. Seto, R. Mari, J. F. Morris, and M. M. Denn, *Discontinuous Shear Thickening of Frictional Hard-Sphere Suspensions*, Phys. Rev. Lett. **111**, 218301 (2013).

[5] R. Mari, R. Seto, J. F. Morris, and M. M. Denn, *Shear Thickening, Frictionless and Frictional Rheologies in Non-Brownian Suspensions*, J. Rheol. **58**, 1693 (2014).

[6] M. Wyart and M. E. Cates, *Discontinuous Shear Thickening without Inertia in Dense Non-Brownian Suspensions*, Phys. Rev. Lett. **112**, 098302 (2014).

[7] N. Y. Lin, C. Ness, M. E. Cates, J. Sun, and I. Cohen, *Tunable Shear Thickening in Suspensions*, Proc. Natl. Acad. Sci. U.S.A. **113**, 10774 (2016).

[8] P. Sehgal, M. Ramaswamy, I. Cohen, and B. J. Kirby, *Using Acoustic Perturbations to Dynamically Tune Shear Thickening in Colloidal Suspensions*, Phys. Rev. Lett. **123**, 128001 (2019).

[9] C. Garat, S. Kiesgen de Richter, P. Lidon, A. Colin, and G. Ovarlez, *Using Good Vibrations: Melting and Controlled Shear Jamming of Dense Granular Suspensions*, J. Rheol. **66**, 237 (2022).

[10] C. Chen, M. van de Naald, A. Singh, N. Dolinski, G. Jackson, H. Jaeger, S. Rowan, and J. de Pablo, *Leveraging the Polymer Glass Transition to Access Thermally-Switchable Shear Jamming Suspensions*, preprint (version 1) available at Research Square [10.21203/rs.3.rs-1193286/v1].

[11] C.-P. Hsu, S. N. Ramakrishna, M. Zanini, N. D. Spencer, and L. Isa, *Roughness-Dependent Tribology Effects on Discontinuous Shear Thickening*, Proc. Natl. Acad. Sci. U.S.A. **115**, 5117 (2018).

[12] C. Hoyle, S. Dai, R. Tanner, and A. Jabbarzadeh, *Effect of Particle Roughness on the Rheology of Suspensions of Hollow Glass Microsphere Particles*, J. Non-Newtonian Fluid Mech. **276**, 104235 (2020).

[13] C.-P. Hsu, J. Mandal, S. N. Ramakrishna, N. D. Spencer, and L. Isa, *Exploring the Roles of Roughness, Friction and Adhesion in Discontinuous Shear Thickening by Means of Thermo-responsive Particles*, Nat. Commun. **12**, 1 (2021).

[14] N. M. James, E. Han, R. A. L. de la Cruz, J. Jureller, and H. M. Jaeger, *Interparticle Hydrogen Bonding Can Elicit Shear Jamming in Dense Suspensions*, Nat. Mater. **17**, 965 (2018).

[15] Y. Moratille, M. Arshad, C. Cohen, A. Maali, E. Lemaire, N. Sintes-Zydowicz, and E. Drockenmuller, *Cross-Linked Polymer Microparticles with Tunable Surface Properties by the Combination of Suspension Free Radical Copolymerization and Click Chemistry*, J. Colloid Interface Sci. **607**, 1687 (2022).

[16] J. A. Richards, R. E. O'Neill, and W. C. Poon, *Turning a Yield-Stress Calcite Suspension into a Shear-Thickening One by Tuning Inter-particle Friction*, Rheol. Acta **60**, 97 (2021).

[17] G. Bossis, Y. Grasselli, and O. Volkova, *Capillary Flow of a Suspension in the Presence of Discontinuous Shear Thickening*, Rheol. Acta **61**, 1 (2021).

[18] J. Comtet, G. Chatté, A. Nigues, L. Bocquet, A. Siria, and A. Colin, *Pairwise Frictional Profile between Particles Determines Discontinuous Shear Thickening Transition in Non-colloidal Suspensions*, Nat. Commun. **8**, 1 (2017).

[19] G. Chatté, J. Comtet, A. Niguès, L. Bocquet, A. Siria, G. Ducouret, F. Lequeux, N. Lenoir, G. Ovarlez, and A. Colin, *Shear Thinning in Non-Brownian Suspensions*, Soft Matter **14**, 879 (2018).

[20] M. Arshad, A. Maali, C. Claudet, L. Lobry, F. Peters, and E. Lemaire, *An Experimental Study on the Role of Interparticle Friction in the Shear-Thinning Behavior of Non-Brownian Suspensions*, Soft Matter **17**, 6088 (2021).

[21] S. Chialvo, J. Sun, and S. Sundaresan, *Bridging the Rheology of Granular Flows in Three Regimes*, Phys. Rev. E **85**, 021305 (2012).

[22] E. DeGiuli, G. Düring, E. Lerner, and M. Wyart, *Unified Theory of Inertial Granular Flows and Non-Brownian Suspensions*, Phys. Rev. E **91**, 062206 (2015).

[23] F. Boyer, É. Guazzelli, and O. Pouliquen, *Unifying Suspension and Granular Rheology*, Phys. Rev. Lett. **107**, 188301 (2011).

[24] É. Guazzelli and O. Pouliquen, *Rheology of Dense Granular Suspensions*, J. Fluid Mech. **852**, P1 (2018).

[25] P. R. Nott and J. F. Brady, *Pressure-Driven Flow of Suspensions: Simulation and Theory*, J. Fluid Mech. **275**, 157 (1994).

[26] A. Deboeuf, G. Gauthier, J. Martin, Y. Yurkovetsky, and J. F. Morris, *Particle Pressure in a Sheared Suspension: A*

Bridge from Osmosis to Granular Dilatancy, Phys. Rev. Lett. **102**, 108301 (2009).

[27] Y. Forterre and O. Pouliquen, *Flows of Dense Granular Media*, Annu. Rev. Fluid Mech. **40**, 1 (2008).

[28] D. Prasad and H. Kytömaa, *Particle Stress and Viscous Compaction during Shear of Dense Suspensions*, Int. J. Multiphase Flow **21**, 775 (1995).

[29] F. Tapia, O. Pouliquen, and É. Guazzelli, *Influence of Surface Roughness on the Rheology of Immersed and Dry Frictional Spheres*, Phys. Rev. Fluids **4**, 104302 (2019).

[30] C. Clavaud, A. Bérut, B. Metzger, and Y. Forterre, *Revealing the Frictional Transition in Shear-Thickening Suspensions*, Proc. Natl. Acad. Sci. U.S.A. **114**, 5147 (2017).

[31] H. Perrin, C. Clavaud, M. Wyart, B. Metzger, and Y. Forterre, *Interparticle Friction Leads to Nonmonotonic Flow Curves and Hysteresis in Viscous Suspensions*, Phys. Rev. X **9**, 031027 (2019).

[32] C. Clavaud, B. Metzger, and Y. Forterre, *The Darcytron: A Pressure-Imposed Device to Probe the Frictional Transition in Shear-Thickening Suspensions*, J. Rheol. **64**, 395 (2020).

[33] T. Loimer, A. Nir, and R. Semiat, *Shear-Induced Corrugation of Free Interfaces in Concentrated Suspensions*, J. Non-Newtonian Fluid Mech. **102**, 115 (2002).

[34] S. Garland, G. Gauthier, J. Martin, and J. Morris, *Normal Stress Measurements in Sheared Non-Brownian Suspensions*, J. Rheol. **57**, 71 (2013).

[35] F. E. Hackett and J. S. Strettan, *The Capillary Pull of an Ideal Soil*, J. Agric. Sci. **18**, 671 (1928).

[36] R. B. Bird, R. C. Armstrong, and O. Hassager, *Dynamics of Polymeric Liquids: Fluid Mechanics* (John Wiley and Sons Inc., New York, 1987), Vol. 1.

[37] T. Dbouk, L. Lobry, and E. Lemaire, *Normal Stresses in Concentrated Non-Brownian Suspensions*, J. Fluid Mech. **715**, 239 (2013).

[38] Note that changes in the volume fraction of the suspension usually result in a global curvature of the air-suspension meniscus, such that an additional capillary term arises in the stress balance at the air-suspension interface [Eq. (1)]: $\sigma_p^r(R) + P_\ell = -2\gamma\cos\theta/h$, where γ is the suspending fluid surface tension and θ the wetting angle of the suspension at the edge of the plate. This term, however, does not affect the measurement of the particle pressure, which is determined from Eq. (2). In practice, adjusting the gap h to keep a constant particle pressure is equivalent to keeping the curvature term constant as set by the initial conditions and maintaining the capillary interface at the edge of plate.

[39] J. N. Israelachvili, *Intermolecular and Surface Forces* (Academic, New York, 2011).

[40] P.-E. Peyneau and J.-N. Roux, *Frictionless Bead Packs Have Macroscopic Friction, but No Dilatancy*, Phys. Rev. E **78**, 011307 (2008).

[41] C. Ness and J. Sun, *Shear Thickening Regimes of Dense Non-Brownian Suspensions*, Soft Matter **12**, 914 (2016).

[42] A. Billon, Y. Forterre, O. Pouliquen, and O. Dauchot, *Transition from Granular to Brownian Suspension: An Inclined Plane Experiment*, arXiv:2209.13239.

[43] M. Wang and J. F. Brady, *Constant Stress and Pressure Rheology of Colloidal Suspensions*, Phys. Rev. Lett. **115**, 158301 (2015).

[44] A. Bérut, O. Pouliquen, and Y. Forterre, *Brownian Granular Flows Down Heaps*, Phys. Rev. Lett. **123**, 248005 (2019).

[45] J. Dong and M. Trulsson, *Analog of Discontinuous Shear Thickening Flows under Confining Pressure*, Phys. Rev. Fluids **2**, 081301(R) (2017).

[46] N. Estrada, E. Azéma, F. Radjai, and A. Taboada, *Identification of Rolling Resistance as a Shape Parameter in Sheared Granular Media*, Phys. Rev. E **84**, 011306 (2011).

[47] A. Singh, C. Ness, R. Seto, J. J. de Pablo, and H. M. Jaeger, *Shear Thickening and Jamming of Dense Suspensions: The "Roll" of Friction*, Phys. Rev. Lett. **124**, 248005 (2020).

[48] L. Berthier, E. Flenner, and G. Szamel, *Glassy Dynamics in Dense Systems of Active Particles*, J. Chem. Phys. **150**, 200901 (2019).

[49] P.-F. Lenne and V. Trivedi, *Sculpting Tissues by Phase Transitions*, Nat. Commun. **13**, 1 (2022).